CATCH ME IF YOU CAN: IS THERE A "RUNAWAY-MASS" BLACK HOLE IN THE ORION NEBULA CLUSTER?

LADISLAV ŠUBR[1], PAVEL KROUPA[2], AND HOLGER BAUMGARDT[3]
[1] Astronomical Institute, Charles University, V Holešovičkách 2, CZ-180 00 Praha, Czech Republic; subr@mbox.troja.mff.cuni.cz
[2] Argelander Institute for Astronomy (AIfA), Auf dem Hügel 71, D-53121 Bonn, Germany
[3] School of Mathematics and Physics, University of Queensland, Brisbane, QLD 4072, Australia

ABSTRACT

We investigate the dynamical evolution of the Orion Nebula Cluster (ONC) by means of direct *N*-body integrations. A large fraction of residual gas was probably expelled when the ONC formed, so we assume that the ONC was much more compact when it formed compared with its current size, in agreement with the embedded cluster radius–mass relation from Marks & Kroupa. Hence, we assume that few-body relaxation played an important role during the initial phase of evolution of the ONC. In particular, three-body interactions among OB stars likely led to their ejection from the cluster and, at the same time, to the formation of a massive object via "runaway" physical stellar collisions. The resulting depletion of the high-mass end of the stellar mass function in the cluster is one of the important points where our models fit the observational data. We speculate that the runaway-mass star may have collapsed directly into a massive black hole ($M_\bullet \gtrsim 100\,M_\odot$). Such a dark object could explain the large velocity dispersion of the four Trapezium stars observed in the ONC core. We further show that the putative massive black hole is likely to be a member of a binary system with ≈70% probability. In such a case, it could be detected either due to short periods of enhanced accretion of stellar winds from the secondary star during pericentre passages, or through a measurement of the motion of the secondary whose velocity would exceed $10\,\mathrm{km\,s^{-1}}$ along the whole orbit.

Key words: black hole physics – stars: kinematics and dynamics – stars: massive

1. INTRODUCTION

The Orion Nebula Cluster (ONC, M42) is a dense star cluster that is part of a complex star-forming region at a distance of about 400 pc (Jeffries 2007; Sandstrom et al. 2007; Menten et al. 2007). Due to its relative proximity, the ONC is one of the best observationally studied star clusters. Its age is estimated to be $\lesssim 3$ Myr, the resolved stellar mass is $M_c \approx 1800\,M_\odot$, and it has a compact core of radius $\lesssim 0.5$ pc (Hillenbrand & Hartmann 1998). Based on the data presented by Huff & Stahler (2006), we estimate a half-mass radius of the cluster of $r_h \approx 0.8$ pc. Hence, the ONC is considered to be a prototype of a dense young star cluster and it naturally serves as a test bed for theoretical models of various astrophysical processes (e.g., Kroupa et al. 2001 considered the dynamical evolution of ONC-type star clusters with gas expulsion; Olczak et al. 2008 studied the destruction of protoplanetary disks due to close stellar encounters).

Nevertheless, the morphological and dynamical state of the ONC is still not fully understood. Some of its characteristics indicate that it has undergone a period of violent evolution and that the current state does not represent a true picture of a newly born star cluster. There is a lack of gas in the cluster (Wilson et al. 1997), which has been expelled due to the radiation pressure of the OB stars that reside in the cluster core. The effect of gas removal is likely to have led to the cluster expanding by a factor $\gtrsim 3$ for a star formation efficiency $\lesssim 50\%$ (e.g., Baumgardt & Kroupa 2007). The assumption that the ONC has been more compact in the past is in accord with the fact that this star cluster is missing wide binaries with separations $> 10^3$ AU, which may have been disrupted through close three-body interactions during the initial compact stage (Kroupa 2000; Parker et al. 2009; Marks & Kroupa 2012). The process of dynamical ejections has been suggested by Pflamm-Altenburg & Kroupa (2006) as a reason for the depletion of the cluster mass function at the high-mass end. This hypothesis aims to explain the observed deficit of massive stars in the ONC (Hillenbrand 1997) with respect to the standard Kroupa (2001) initial mass function (IMF). Finally, observations (Zapata et al. 2009) have brought evidence that stellar disruptions occurred in the ONC recently. These may be a consequence of physical stellar collisions in the dense cluster core.

In this paper we address the history of the ONC over its lifetime. We concentrate on initially very compact star clusters and show that they can evolve within a few million years into a state compatible with the current observations. In particular, we address the fact that the central system of OB stars, the so-called Trapezium, is super-virial and, at the same time, that the ONC hosts unexpectedly few OB stars.

2. MODEL

We restricted ourselves to the stage of cluster evolution when the stars have already formed as individual entities that can be characterized by a constant mass and radius. Stellar dynamics is then driven mainly by gravitational interactions. We used the numerical code NBODY6 (Aarseth 2003), which is a suitable tool for modeling self-gravitating stellar systems with a considerable amount of binaries.

At the initial stage of its evolution, a substantial contribution to the gravitational field of the cluster is due to gas. We incorporated external gas into our model by means of a special type of low-mass particles ($m_g \leqslant 0.4\,M_\odot$) whose gravitational interaction with the rest of the cluster was treated directly via the *N*-body scheme. Beside that, we modified the original NBODY6 code, including an option for a *repulsive* force (with the direction radial from the cluster center) acting upon the gas particles in order to mimic the radiation pressure from the stars starting

at a given time T_{ex} (see Section 3.2). Alternatively, we also modeled the gas expulsion by an instantaneous removal of the gas particles at a given time.

Stellar masses were calculated according to the Kroupa (2001) mass function with an upper mass limit of $80 M_\odot$ (however, the mass of the most massive star is typically $\approx 63 M_\odot$). For several numerical reasons (e.g., quadratic growth of CPU time with the number of particles, higher probability of numerical errors for extreme mass ratios), we replaced low-mass stars ($M_\star \leqslant m_{min}$) by stars with mass m_{min}, keeping the total mass unchanged. We have verified (cf. models 4 and 6 introduced below, which have $m_{min} = 0.5 M_\odot$ and $0.2 M_\odot$, respectively) that our results are not affected considerably by this approximation.

The stars were considered to have finite radii $R_\star = R_\odot (M_\star/M_\odot)^{0.8}$ (e.g., Lang 1980; this simple formula also fits well the radii of zero-age main-sequence stars for $M_\star \gtrsim M_\odot$ according to Eggleton et al. 1989; our overestimation of stellar radii for $M_\star \lesssim M_\odot$ does not affect our results, as the low-mass stars contribute only marginally to the merging tree). If the separation of two stars got below the sum of their radii, they were merged into a single star. We also switched off the option of stellar evolution in the numerical code. Loss of realism is assumed to be negligible as we followed the cluster evolution for a period of only 2.5 Myr. The stars in our models are not assigned a spectral type. For the sake of brevity, we refer to all stars with $M_\star \geqslant 5 M_\odot$ as "OB stars."

2.1. The "Canonical" Model

The canonical (best-fit) model of the ONC has an initial mass of $5400 M_\odot$, half of which is in the form of stars, while gas accounts for the other half. We considered a Kroupa (2001) IMF, which, for the given cluster star mass, predicts ≈ 50 OB stars to have been formed in the ONC (Pflamm-Altenburg & Kroupa 2006). In order to avoid additional statistical noise in the evolution of the number of OB stars, we used identical samples of stellar masses for all numerical realizations of the model. The initial half-mass radius of the cluster is $r_h \approx 0.11$ pc, which is compatible with the initial or birth radius–mass relation inferred for star clusters ranging in mass up to globular clusters (Marks & Kroupa 2012). Positions and velocities are generated in a mass segregated state according to the prescription of Šubr et al. (2008) with mass segregation index $S = 0.4$. The algorithm by definition places massive stars in the cluster core and, therefore, the initial half-mass radius of the OB stars is ≈ 0.05 pc. In order *not* to place the light gas particles at the cluster outskirts, we generated initial positions for stellar and gas particles separately, i.e., we had a constant gas to star mass ratio throughout the whole cluster at $T = 0$. All OB stars were set to be members of primordial binaries with a secondary mass $M_s \geqslant 1 M_\odot$ with the pairing algorithm being biased toward assigning a massive secondary to a massive primary. More specifically, the algorithm first sorts the stars from the most massive to the lightest one. The most massive star from the set is taken as the primary. The secondary star index, id, in the ordered set is generated as a random number with the probability density $\propto$ id$^{-\beta}$ and max(id) corresponding to a certain mass limit, $M_{s,min}$. The two stars are removed from the set and the whole procedure is repeated until stars with $M_\star \geqslant M_{p,min}$ remain. Typically, we used as the minimal mass of the primary $M_{p,min} = 5 M_\odot$, as the minimal mass of the secondary $M_{s,min} = 1 M_\odot$ and the pairing algorithm index $\beta = 40$. For the assigned binaries we used a semimajor axis distribution according to Öpik's
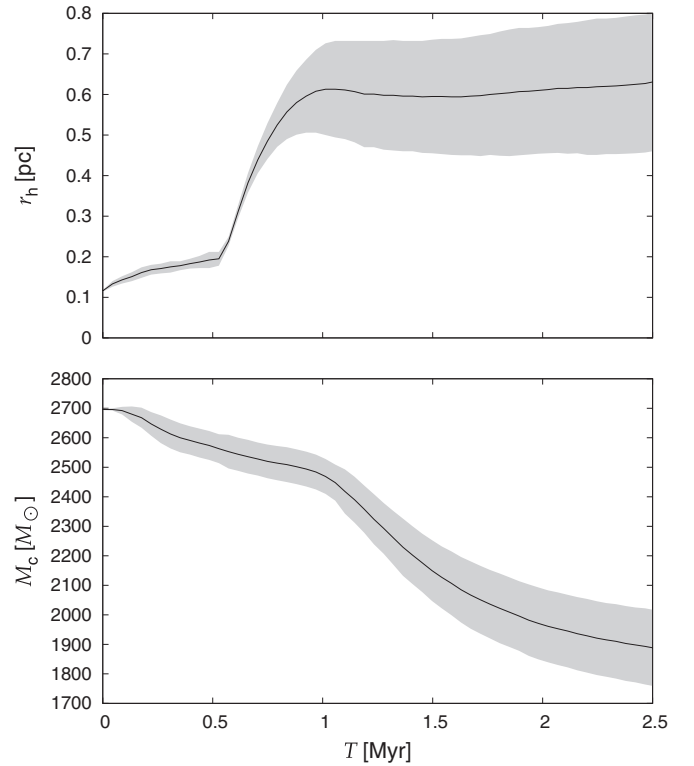

Figure 1. Half-mass radius of the star cluster of our canonical model of the ONC (upper panel). Expansion is accelerated at $T \approx 0.5$ Myr due to gas expulsion. The total mass of the stars within a 3 pc radius (lower panel) monotonically decreases as stars escape out of the observer's field of view. This curve reflects gas expulsion with a time delay of ≈ 0.5 Myr, which is the time the stars need to reach the 3 pc boundary. The shaded area represents the 1σ variance of the individual realizations of the model.

law $n(a) \propto a^{-1}$ (Kobulnicky & Fryer 2007) and a thermal distribution of eccentricities, $n(e) \propto e$. Except for the possibility of being a secondary member of a binary containing an OB star, we did not generate binaries of low-mass stars. This limitation comes from the requirement of numerical effectivity and it is not likely to affect our results substantially.

Let us note that the canonical model presented above fits into the range of the expanding class of models of the ONC discussed by Kroupa (2000). Other possible initial conditions would be fractal models that collapse (e.g., Allison et al. 2010). These require star formation to be synchronized across the pre-cluster cloud core to much shorter than the dynamical time though.

2.2. Dynamical Evolution

Most of the features of the evolution of a star cluster with strong few-body relaxation and gas expulsion can be demonstrated with the canonical model. In order to distinguish systematic effects from rather large fluctuations of cluster parameters, we present quantities averaged over 100 realizations of the model. The upper panel of Figure 1 shows the temporal evolution of the half-mass radius of the stellar component, r_h. During the initial phase, the cluster expands due to two-body relaxation. Gas expulsion that starts at $T_{ex} = 0.5$ Myr removes all gas from the cluster within a few hundred thousand years. From the point of view of the stars, this event leads to an abrupt decrease of their potential energy. Consequently, they can reach larger distances from the cluster center, which manifests itself as an accelerated growth of r_h at 0.5 Myr $\lesssim T \lesssim 1$ Myr. Initially

weakly bound stars became unbound due to the gas expulsion and they escape from the cluster. Hence, reduction of the cluster mass also accelerates—see the lower panel of Figure 1 where we plot the mass of the star cluster. We define M_c as the sum of the mass of the stars within a sphere of radius r_{lim} from the cluster center. We set $r_{lim} = 3\,pc$ in order to match typical observations of the ONC, which usually count stars within a projected distance of $\approx 3\,pc$ from the Trapezium. Note that the decrease of M_c is accelerated with $\approx 0.5\,Myr$ delay after the time of gas expulsion. This is due to the unbound stars taking some time to reach r_{lim}. Besides the escape of stars due to the gas expulsion, there is also continuous stellar mass loss due to the few-body relaxation, which is capable of accelerating stars above the escape velocity. From $T \approx 1\,Myr$ onward the cluster expansion is again dominated by relaxational processes driving a revirialization (Kroupa et al. 2001).

Our model indicates that the initial mass of the ONC must have been at least 20% larger than it is now, after a few million years of dynamical evolution. We also see that, mainly due to the effect of gas expulsion, the ONC must have been more compact by a factor $\gtrsim 5$ at the time of its birth than it is now. Hence, the initial relaxation time was much shorter than what we would infer from present-day observations. Consequently, close few-body interactions must have been more frequent in the past. In particular, we suggest that scattering of single stars on binaries is a process that has played an important role in the evolution of the ONC. This kind of interaction has been studied intensively in the literature (e.g., Heggie & Hut 2003 and references therein). A rich variety of outcomes can be obtained, depending on the initial conditions. Nevertheless, some general results can be formulated. In particular, if the binary is hard, i.e., its orbital velocity is larger than the impact velocity of the third star, it typically shrinks, losing its energy, which is transferred to the accelerated single star. Therefore, we expect two processes to happen in correlation: (1) ejections of high-velocity stars and (2) physical collisions of massive binaries, which lead to the formation of more massive objects.

The probability of collisions increases with the mass of the interacting stars. Therefore, numerical models by different authors often show a "runaway" process when most of the collisions involve the most massive object which grows continuously (e.g., Portegies-Zwart et al. 2004). The same is true also for our model of the ONC. The upper panel of Figure 2 shows the growth of the mass of the most massive object, $M_\bullet$, due to stellar collisions; the number of OB stars left in the cluster is plotted in the lower panel. Approximately, one third of the missing OB stars have disappeared due to merging, while the other two thirds have been ejected from the cluster with velocities $>10\,km\,s^{-1}$. The merging tree varies significantly among individual realizations of the particular model. In general, more than one merging star is formed during the initial $\approx 0.5\,Myr$. Among other processes, this is due to the merging of several primordial OB binaries. At later stages, usually one runaway-mass object dominates the merging process.

In the Appendix we provide an approximate description of the rate of stellar ejections due to the scattering of single stars on massive binaries. It gives an estimate of the decay time of the number of the OB stars of $\tau \gtrsim 5\,Myr$ for the canonical model. If we assume that the decay rate is linearly proportional to the number of OB stars, we expect roughly an exponential decay of N_{OB}, i.e., it should reach half of its initial value at $\sim 3.5\,Myr$, which is in good agreement with the numerical results.
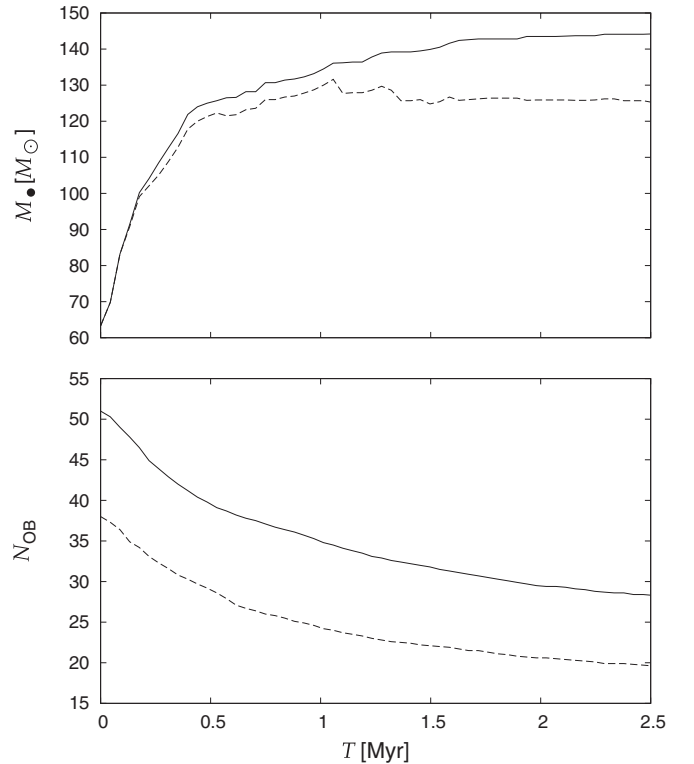

Figure 2. Top: mean mass of the most massive (collisional) star in the model regardless of its location (solid line) and mean mass of the most massive star within 3 pc from the cluster center (dashed line). Bottom: number of OB stars (solid line) and number of OB systems (dashed line) within 3 pc from the cluster center.

A mean number of OB stars of ≈ 28 remain at $T = 2.5\,Myr$. This considerably exceeds the number of OB systems observed in the ONC—the study of Hillenbrand (1997) reports only 10 stars heavier than $5\,M_\odot$. However, the real number of massive stars may be somewhat larger due to their "hiding" in OB binary systems. Our models always end up with several OB stars having an OB companion and, therefore, a better agreement with the observations is achieved if we count the OB *systems* as indicated with the dashed line in Figure 2. Moreover, due to the stochastic nature of dynamical cluster evolution, different realizations of the model end up with quite different values of N_{OB} and $M_\bullet$. The final state ($T = 2.5\,Myr$) of all realizations of the canonical model is shown in Figure 3. Although the distribution of points in the N_{OB}–$M_\bullet$ space is rather noisy, we can deduce an anticorrelation between these two quantities (their linear correlation coefficient is -0.42). In particular, *all* realizations that end up with $N_{OB} \leqslant 20$ lead to the formation of a runaway-mass star of mass $M_\bullet > 100\,M_\odot$. In other words, the underabundance of the high-mass stars in the ONC not only indicates a period of prominent two-body relaxation in the past, but also the merging formation of a massive object that may represent an important footprint of the cluster's history.

Interestingly, the term "runaway" has a secondary meaning in some cases. Despite of its high mass, in several realizations the merging object has been ejected out of the cluster with velocity exceeding $10\,km\,s^{-1}$. These cases can be identified due to differences of the upper and lower panels of Figure 3. The escape of the most massive body beyond the 3 pc boundary is also responsible for the drops of the dashed line in the plot of the temporal evolution of $M_\bullet$ in Figure 2, which shows the mean
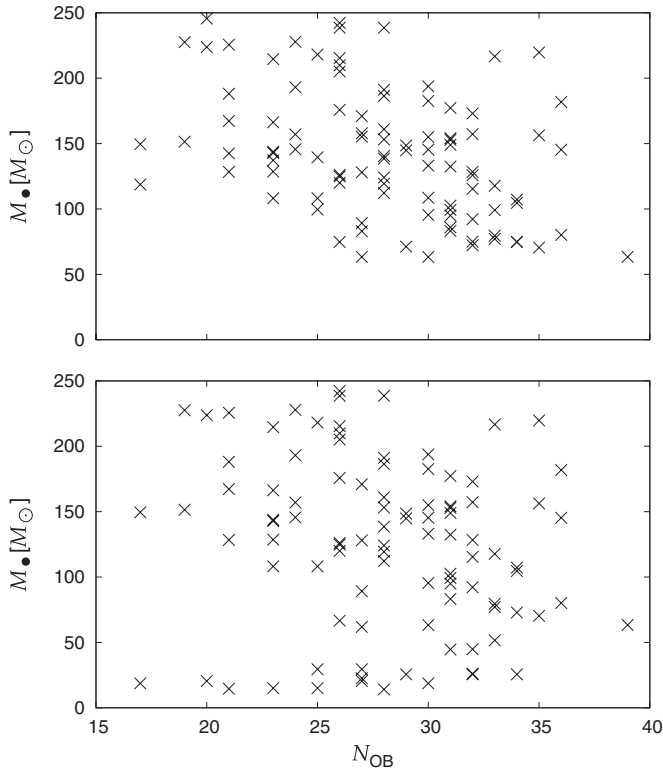
Figure 3. Mass of the most massive object in the cluster vs. the number of OB stars within a radius of 3 pc. Individual points represent states of different realizations of the canonical model at $T = 2.5$ Myr. Mass of the most massive object in the whole set is plotted in the upper panel, while in the lower one, only objects found within 3 pc are considered.

mass of the most massive object within 3 pc from the cluster center.

3. DISCUSSION

The final state of the canonical model presented in the previous section matches basic observables of the ONC quite well, in particular its mass and half-mass radius. The mean number of OB stars is somewhat larger than what is observed in the ONC, nevertheless, some of the realizations reach $N_{OB} < 20$. Hence, we consider this model to be a realistic representation of the ONC. We have investigated several tens of different models with different values of the parameters including the index of the initial mass segregation, initial half-mass radius, mass of the cluster, star to gas mass fraction, and the time of the gas expulsion. Models whose final state can be considered compatible with the current state of the ONC, at least in some of their characteristics, are listed in Table 1.

3.1. N_{OB}–$M_\bullet$ Anticorrelation

As mentioned above, the canonical model indicates an anticorrelation between the final number of the OB stars and the final mass of the runaway-mass star. In Figure 4 we plot the mean mass of the most massive object versus the mean number of remaining OB stars for all models listed in Table 1. Now, each point represents an average over several tens of realizations of the particular model and an N_{OB}–$M_\bullet$ anticorrelation becomes evident. We attribute this relation to the fact that both mechanisms of OB star removal, i.e., physical collisions and ejections, are driven by a common underlying process of close
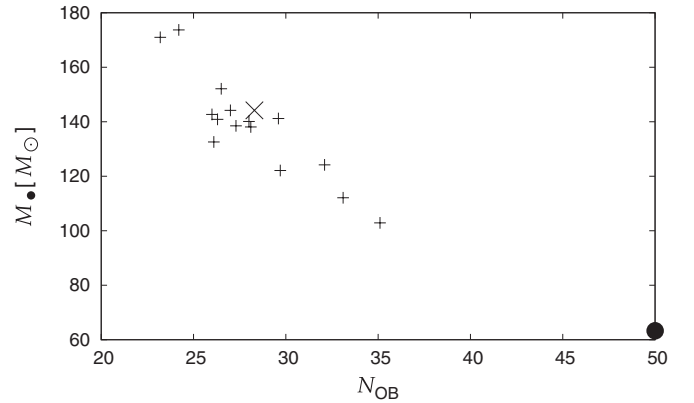

Figure 4. Mean mass of the most massive object in the cluster vs. the mean number of OB stars (both within 3 pc) at $T = 2.5$ Myr for several different models of compact star clusters listed in Table 1. The canonical model is represented with the × sign; full circle stands for the initial state, which is common for all models.

Table 1
Initial Parameters and Final States of Several Models

id	S	$T_{ex}/$Myr	ϵ	$r_h/$pc	$M_c/M_\odot$	N_{OB}	$M_\bullet/M_\odot$
1	0.00	0.5	0.50c	0.56	2183	35.1	102.9
2	0.00	0.7	0.50c	0.48	2061	28.1	138.1
3	0.25	0.7	0.50c	0.51	1980	26.2	140.9
4	0.40	0.5	0.50c	0.59	1895	28.0	140.1
5	0.40	0.5	0.50c	0.60	1938	27.3	138.5
6	0.40	0.5	0.50c	0.63	1887	28.3	144.2
7	0.40	0.5	0.50c	0.66	1660	26.0	142.7
8	0.40	0.5	0.50v	0.47	2197	29.7	122.1
9	0.40	0.7	0.50c	0.62	1895	26.5	152.1
10	0.40	0.7	0.50c	0.58	1882	27.0	144.2
11	0.40	0.7	0.50c	0.67	1636	26.1	132.6
12	0.00	0.7	0.33c	0.52	1717	24.2	173.7
13	0.25	0.5	0.33v	0.51	2109	32.1	124.2
14	0.40	0.5	0.33v	0.50	2196	33.1	112.1
15	0.40	0.5	0.33c	0.77	1300	23.2	171.0

Notes. Common initial parameters of all models are the initial mass of the stellar component, $M_c = 2700\,M_\odot$ which implies $N_{OB}(T = 0) = 50$ and $M_\bullet(T = 0) \approx 63\,M_\odot$. The initial half-mass radius varies slightly throughout the models, but is generally ≈ 0.1 pc. The gas particles are of mass $0.2\,M_\odot$ for models 6 and 10; in all other cases $m_{gas} = 0.4\,M_\odot$ is considered. In models 7 and 11, gas particles were removed instantaneously at $T = T_{ex}$; in all other cases, T_{ex} is the time when the repulsive force was switched on. S is the mass segregation index as defined in Šubr et al. (2008). $\epsilon \equiv M_c/(M_c + M_{gas})$ is the star formation efficiency; suffix "c" stands for constant ϵ throughout the whole cluster, while "v" means variable ϵ (decreasing outward). Öpik's distribution of semimajor axes of the primordial binaries is considered in all models except for 5, where we set $n(a) = $ const. The canonical model has id 6.

three-body interactions (see the Appendix). Naturally, their importance grows with increasing stellar density. Hence, the models that stay more compact during the course of their evolution are located in the top-left corner of the graph. They better fit the observations from the point of view of the number of OB stars, however, either their half-mass radius or total stellar mass at $T = 2.5$ Myr is too small, i.e., not consistent with the observations.

3.2. Gas Expulsion

In most of our models, the gas particles were blown out of the cluster due to a repulsive external force $\propto r/r^3$ centered on the cluster core. The strength of the force was set such that the

Table 2
Comparison of Models with Different Masses of Gas Particles

m_g	N_{OB}	$M_\bullet$	N_{run}	$P_{KS,N_{OB}}$	$P_{KS,M_\bullet}$	Comment
0.40	39.7	125.1	40	95%	42%	Model 4
0.20	39.8	124.9	100	$\cdots$	$\cdots$	Canonical model
0.05	38.2	128.5	14	82%	87%	
0.03	39.9	126.7	14	32%	75%	

Notes. Mean values of the number of OB stars within the radius of 3 pc from the cluster center, N_{OB}, and mass of the runaway-mass star, $M_\bullet$, for models with different values of m_g. All other parameters of the models, including the total mass of gas, are identical to the canonical model. $P_{KS,*}$ is the Kolmogorov–Smirnov probability that the null hypothesis (assuming the particular data set comes from the same distribution as the canonical one) is valid. Note that a value of $P_{KS,*} \approx 5\%$ is usually considered to be a limit below which the null hypothesis should be rejected.

gas particles were accelerated to velocities $\approx 8 \, \mathrm{km \, s^{-1}}$ on the timescale of ≈ 0.1 Myr. This approach is the most realistic one, keeping the continuity equation fulfilled, but, at the same time, it is numerically the most expensive. The alternative method with instantaneous removal of the gas particles at T_{ex} leads to similar results. The clusters integrated with this method typically result in somewhat lower total mass and larger half-mass radius at the final time. Let us note, for completeness, that in the literature, another method that mimics gas removal in numerical models of star clusters is also used (e.g., Geyer & Burkert 2001; Kroupa et al. 2001; Baumgardt & Klessen 2011). It is based on the time-variable smooth external potential that represents the weakening gravitational potential of the gas. It has been found that the two approaches (i.e., modeling gas via particles versus external potential) lead to nearly indistinguishable results (Geyer & Burkert 2001). In order to check for a possible bias of our gas particles approach that may stem from two-body relaxational processes, we have integrated two additional models with very low masses for the gas particles. Due to the large number of particles in these integrations, we have followed their evolution only up to the time of the gas expulsion, $T_{ex} = 0.5$ Myr. Outcomes of these models in terms of the mean number of remaining OB stars, N_{OB}, and the mass of the runaway-mass star, $M_\bullet$, are presented in Table 2. Besides just giving the mean values of N_{OB} and $M_\bullet$, we have also performed a Kolmogorov–Smirnov test comparing the sets of N_{OB} and $M_\bullet$ coming from these models with the canonical one. As can be seen, there is no apparent dependence of the results on m_{gas} ranging from 0.03 to $0.4 \, M_\odot$. Hence, we conclude that the two-body relaxation due to the gas particles does not play a significant role in our simulations.

The evolution of the radiation pressure in the real ONC has been definitely more complicated. According to observations (Huff & Stahler 2006), the star formation in the ONC was continuous with the most massive stars starting to be formed no more than 2 Myr ago. Setting T_{ex} in our models to either 0.5 or 0.7 Myr appears to have only a marginal impact on the final state of the cluster. Hence, we assume that a more complicated temporal prescription of the gas removal would not affect our results considerably.

3.3. The Runaway-mass Star or Black Hole

Under the assumption of an invariant canonical IMF and a small initial cluster radius, the formation of the runaway-mass object via stellar collisions appears to be an inevitable process that, together with the high-velocity ejections, decreases the

number of OB stars in a dense star cluster. Its possible detection would definitely strongly support the scenario of the ONC history presented in this paper.

The current state of the runaway-mass star is, however, not clear. The massive star would definitely have undergone a fast internal evolution. While successive merging events may lead to very fast mass growth, stellar winds act in the opposite way. The state of the runaway-mass object after ≈ 2 Myr of evolution depends on the (dis)balance of these two processes. In the literature, quite different predictions on this subject can be found. Glebbeek et al. (2009) suggest that winds should work in a self-regulatory manner, limiting the maximum mass and, consequently the star's lifetime. Other authors (e.g., Suzuki et al. 2007; Pauldrach et al. 2011) state that stellar winds of the runaway-mass star will not be able to terminate its growth and it may then collapse to a massive black hole. There is no observational evidence for a star with a mass above $50 \, M_\odot$ in the ONC that could be interpreted as a runaway-mass object. The most massive stellar member of the ONC, Θ^1C, is a binary with a total mass of about $45 \, M_\odot$ and mass ratio ≈ 0.25 (Kraus et al. 2009), i.e., the primary has mass $\lesssim 35 \, M_\odot$. It does not exhibit a stellar wind strong enough to reduce its mass by several tens of $M_\odot$. Hence, our scenario assumes a low efficiency of stellar winds, i.e., continuous growth of the runaway-mass star, which forms a massive black hole at the end of its lifetime. There is no general consensus regarding whether the collapse of a star more massive than $150 \, M_\odot$ will be followed by an ejection of most of its mass. As there is no evidence for a supernova remnant in the ONC, we assume most of the mass of the runaway-mass star, if it is present, to have collapsed directly into a black hole.

The putative black hole in the ONC would be detectable only through an interaction with its environment. One possibility is an accretion of surrounding gas, which could be detectable through X-ray radiation. The main source of the gas in the Trapezium region is stellar winds from the remaining OB stars. We estimate that they produce at most $10^{-5} \, M_\odot \, \mathrm{yr^{-1}}$ within the central 0.2 pc. However, the black hole is likely to capture only the gas that falls within its Bondi radius ≈ 100 AU, i.e., the accretion rate could be $\lesssim 10^{-15} \, M_\odot \, \mathrm{yr^{-1}}$. Such a highly sub-Eddington accretion will not be detectable in the region confused with several X-ray young stellar sources.

A better chance for detecting the black hole would be given if it is a member of a binary. This indeed appears to be the case for about two thirds of the realizations of the canonical model. However, the typical separation of the black hole and the secondary appears to be from several tens to hundreds of AU (see Figure 5). Even with the relatively large eccentricities achieved, in no case does the secondary star fill its Roche radius at the pericentre of its orbit, i.e., we do not expect the black hole to be a member of a mass transferring system. Still there would be a chance for a detectable accretion provided the secondary star is massive ($M_\star \gtrsim 10 \, M_\odot$). In such a case, its stellar wind may produce short periods of enhanced activity during pericentre passages, but the corresponding luminosity is rather uncertain. Let us consider the well known Cyg-X1 system as a kind of template. Having a black hole mass of $\approx 10 \, M_\odot$ and separation from the secondary star of ≈ 0.2 AU, it has a luminosity $\approx 2 \times 10^{37} \, \mathrm{erg \, s^{-1}}$ (Wilms et al. 2006), which corresponds to $\approx 10^{-4}$ of the rest-mass energy of the winds emitted by the secondary star ($\approx 10^{-6} \, M_\odot \, \mathrm{yr^{-1}}$). Assuming the same effectivity in conversion of the stellar winds into radiation, we estimate the luminosity to be similar to the Cyg-X1 system,
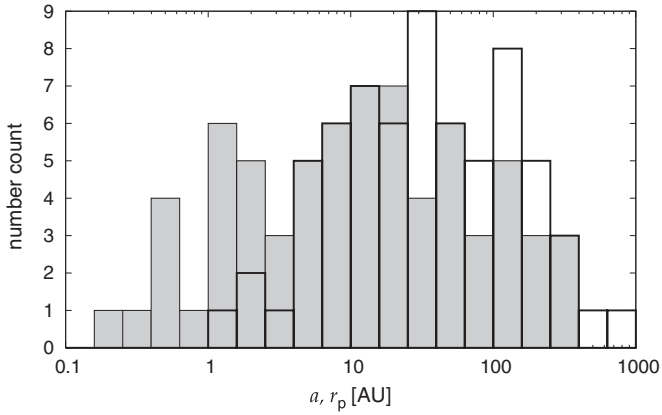
Figure 5. Histogram of the semimajor axes (*a*, empty boxes) and pericentre distances (*r*$_p$, full boxes) of the binaries involving the runaway-mass star in the canonical model. A total of 100 runs were examined, out of which 70 harbor the runaway-mass star with a stellar companion (three of them with $a > 1000$ AU).

i.e., $\approx 10^4 \, L_\odot$, for separations of the order of 1 AU. Considering the density of the stellar wind to decrease with the square of the distance, we obtain a rough estimate of the peak luminosity $L \approx 10^4 (r_p/1 \, \mathrm{AU})^{-2} \, L_\odot$. According to the mass of the putative black hole, the maximum of the emitted radiation is expected to lie in the X-ray band. The accretion events should be recurrent with a period ranging from years to hundreds of years. A shorter period generally implies a smaller r_p, i.e., larger values of the peak luminosity.

3.4. Velocity Dispersion

Another way of an indirect detection of the massive black hole in the ONC lies in velocity dispersion measurements. It has been stated by several authors that the core of the ONC ($r \lesssim 0.25$ pc) is dynamically hot with a velocity dispersion $\gtrsim 4 \, \mathrm{km \, s^{-1}}$ (e.g., Jones & Walker 1988; van Altena et al. 1988; Tobin et al. 2009). The missing stellar mass required for virial equilibrium in the innermost region of the ONC was estimated to be $\gtrsim 2000 \, M_\odot$ which exceeds the observed mass $\approx 200 \, M_\odot$ by an order of magnitude. Kroupa et al. (2001) demonstrate that the globally super-virial velocity dispersion is readily obtained if the ONC is expanding now after expulsion of its residual gas, but some of the missing mass in the inner region could be attributed to the invisible remnant of the runaway-mass star.

As we show in Figure 6, our canonical model gives a velocity dispersion $\gtrsim 4 \, \mathrm{km \, s^{-1}}$ in the inner 0.25 pc, which is in accord with the observational data. In order to inspect the influence of the mass of the runaway-mass object on the velocity dispersion, we have divided the 100 realizations of the canonical model into two groups of 50 according to the mass of the most massive object that remained in the cluster. It appears that the clusters with $M_\bullet \gtrsim 120 \, M_\odot$ have a velocity dispersion within 0.25 pc somewhat larger than those with $M_\bullet \lesssim 120 \, M_\odot$, nevertheless, even within the latter group we have $\sigma \gtrsim 3.5 \, \mathrm{km \, s^{-1}}$, i.e., an apparently super-virial core region. Together with the fact that none of our numerical experiments led to $M_\bullet \gtrsim 2000 \, M_\odot$, virtually required by the condition of virial equilibrium, this indicates that the large velocity dispersion can be only partly due to the hidden mass of the runaway-mass object. Detailed analysis of our models shows that there are two other reasons for having large velocity dispersion in the core. First, according to our models, the ONC is a post-core-collapse cluster with centrally
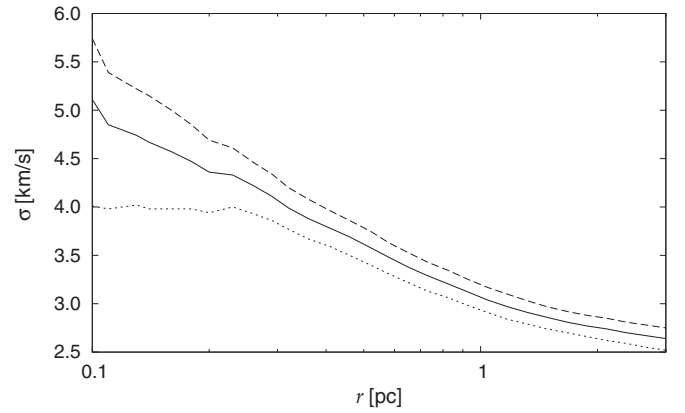

Figure 6. Velocity dispersion σ within a specified radius r at the final state of the canonical model. For distinguished bound multiple systems, the center-of-mass velocity is counted instead of the proper velocities of the individual components. Solid line represents the average over all realizations; thin dashed line corresponds to half of the computations yielding more massive ($M_\bullet \gtrsim 120 \, M_\odot$) runaway-mass object, while the dotted line stands for the computations with lower $M_\bullet$.

Table 3
Trapezium Stars Data

Name	$M/M_\odot$	$v_{\mathrm{los}}/\mathrm{km \, s^{-1}}$
$\Theta^1 A$	18.9	33.4 ± 2
$\Theta^1 B$	7.2	24.0 ± 2
$\Theta^1 C$	44 ± 7	23.6
$\Theta^1 D$	16.6	32.4 ± 1

Notes. Stellar masses of $\Theta^1 A$, $\Theta^1 B$, and $\Theta^1 D$ are taken from Hillenbrand (1997). Radial velocity data of $\Theta^1 A$ and $\Theta^1 B$ come from the C.D.S.—SIMBAD database; data of $\Theta^1 D$ follow Vitrichenko (2002). Both mass and radial velocity of $\Theta^1 C$ are according to Kraus et al. (2009).

peaked density. This leads to a deep gravitational potential well that allows the central velocity dispersion to be larger than what would be expected, e.g., for the Plummer profile. Second, in our models and perhaps also in the real ONC, there are likely to be present several unidentified wide binaries with orbital velocities exceeding $10 \, \mathrm{km \, s^{-1}}$, which affect the velocity dispersion.

Figure 6 indicates that the presence of the dark massive body influences remarkably (i.e., by more than $1 \, \mathrm{km \, s^{-1}}$) the velocity dispersion in a small region of a radius of ≈ 0.1 pc. This is in accord with an analytical estimate of the influence radius of the black hole, $r_h = GM_\bullet/\sigma^2$, which for $M_\bullet = 100 \, M_\odot$ and $\sigma = 3 \, \mathrm{km \, s^{-1}}$ gives $r_h \approx 0.05$ pc. Due to the small number count of stars in such a small region, standard statistical methods do not represent a robust tool for determining the presence of a dark massive body. Nevertheless, having this caution in mind, let us discuss the velocity dispersion of the compact core of the ONC, the four Trapezium stars. According to the published observational data (see Table 3), the line-of-sight velocity dispersion of the Trapezium is $\sigma_{\mathrm{los}} \approx 4.6 \, \mathrm{km \, s^{-1}}$, which implies a three-dimensional velocity dispersion $\sigma \approx 7.9 \, \mathrm{km \, s^{-1}}$. Considering a sphere of radius $r_T \approx 0.025$ pc covering the four Trapezium stars, we obtain an estimate of the enclosed mass required for the system to be in virial equilibrium: $M_{\mathrm{bind}} \approx r_T \sigma^2/G \approx 350 \, M_\odot$. Taking into account the stellar mass of the Trapezium ($\approx 90 \, M_\odot$), we find it to be an apparently dynamically very hot system. Our models suggest that the

virial equilibrium state can be achieved by the presence of the runaway-mass object.

Yet another, and statistically better founded, argument for a hidden massive body comes from the comparison of the kinematical state of the Trapezium and similar subsystems found in our numerical models. We have implemented an algorithm similar to that used by Allison & Goodwin (2011) for detection of Trapezium-like systems. In particular, for each OB star we determined its three nearest OB neighbors (either single OB stars, or bound systems containing at least one OB star). The set of stars was considered Trapezium-like if all members had the same OB neighbors. In order to obtain a statistically significant sample, we examined the last 20 snapshots (covering the period from ≈1.5 Myr to 2.5 Myr) of 100 independent realizations of the canonical model. We found Trapezium-like systems in a third of cluster snapshots. The mean value of the velocity dispersion of these systems was found to be ≈7.5 km s^{-1}. The runaway-mass star was excluded from the search algorithm. Furthermore, we have distinguished systems according to their center of mass distance to the runaway-mass object. In approximately two thirds of the Trapezium-like systems, the runaway-mass object was found within a distance smaller than max(Δr_{ij}), with Δr_{ij} denoting separations of individual members. The mean velocity dispersion of the Trapezium-like system of this subset was ≈9.0 km s^{-1}, while it was only ≈4.3 km s^{-1} for the remaining cases.

Finally, let us remark that kinematical evidence of a massive black hole in the ONC may also lie in the ≈70% probability that it is a member of a binary (see Section 3.3). The typical velocity of the secondary star should be >10 km s^{-1}, i.e., considerably exceeding the observed central velocity dispersion.

4. CONCLUSIONS

We have carried out extensive modeling of the dynamical evolution of compact young star clusters, aiming to reconstruct the history of the ONC. Assuming that the ONC underwent primordial gas expulsion, we have shown that the ONC must have been several times more compact than it is now, in agreement with Kroupa (2000) and Kroupa et al. (2001). This implies that its two-body relaxation time was considerably shorter in the past and, consequently, that close few-body interactions between massive stars were rather frequent. We have concentrated on two significant tracks of such interactions that lead either to high-velocity ejections of massive stars from the cluster or to their physical collisions that are likely to lead to the formation of a massive "runaway" merging object. Both of these processes decrease the number of massive stars in the cluster. Hence, the observed significant lack of massive OB stars in the ONC further supports our assumption that this star cluster has undergone a relaxation-dominated period since its birth.

We have shown that it is not unfeasible that the center of the ONC harbors a black hole of mass ≳100 $M_\odot$ as the remnant of the massive runaway-mass star. Its presence could be revealed either by episodic accretion events or by a thorough kinematical study of the innermost ≈0.05 pc region of the ONC, where the hidden mass would increase the velocity dispersion above 5 km s^{-1}. In particular, we have shown that the observed velocity dispersion of the Trapezium system can be achieved by the presence of an object of mass ≈150 $M_\odot$ which is fully consistent with the hypothesis of the runaway-mass object. Our model also shows that the apparent super-viriality of the central ≈0.25 pc can be explained as a natural attribute of a post-core-collapse dynamical state of a star cluster with a considerable binary fraction.

The possible detection of the remnant of the merger object could bring new light into several fields of contemporary astrophysics. First, it would confirm the hypothesis that star clusters similar to the ONC are being formed very compact with a half-mass radius of the order of a few tenths of a parsec (Marks & Kroupa 2012). Second, and probably more importantly, it would have important implications for the evolution of very massive stars and merger products for which we have only a limited understanding now.

APPENDIX

THEORETICAL PREDICTIONS

Unlike two-body relaxation, interactions among three or more stars allow considerable energy transfer from one component to another. Therefore, multiple-body scattering is essential for both processes (merging and ejections) that lead to the reduction of the number of massive stars in the cluster. In spite of the chaotic nature of the dynamical evolution of the star cluster core, it is possible to derive a raw estimate of the rate of OB stars ejections and collisions.

Our approximation of three-body scattering follows the work of Perets & Šubr (2012): Consider an interaction of a binary of mass $M_B = M_1 + M_2$ and a single star $M_\star$. Large accelerations of the single star are assumed to occur when it passes around one of the binary components within the semimajor axis, a, of the binary. The cross-section of the interaction is assumed to be determined by gravitational focusing:

$$\Sigma(a) \approx \frac{2\pi G M_B a}{v_c^2}, \tag{A1}$$

where v_c is the characteristic stellar velocity in the cluster and G stands for the gravitational constant.

The energy transfer estimate is based on the approximation that the impacting star moves along a hyperbolic orbit around M_1 perturbed by M_2. The typical perturbing force is

$$F \approx \frac{G M_2 M_\star}{a^2} \tag{A2}$$

and it acts along the star's trajectory segment of length $\approx a$. Hence, the energy transfer to the star is

$$\Delta E_\star \approx \frac{G M_2 M_\star}{a} \approx \frac{G M_B M_\star}{a}. \tag{A3}$$

Here we for simplicity assume the mass of the binary to be of the same order as the mass of the secondary, $M_B \approx M_2$. In the cases when $\Delta E_\star$ is much larger or at least comparable to the star's energy before the interaction, it will be accelerated to

$$v_{acc} \approx \sqrt{\frac{2 G M_B}{a}}. \tag{A4}$$

Finally, let us assume the distributions of the binary mass, semimajor axis, and eccentricity in a simple power-law form,

$$n(a, e, M_B) = 2A \, e \, a^{-1} \, M_B^{-\alpha} \tag{A5}$$

in the interval $a \in \langle a_{min}, a_{max}\rangle$, $e \in \langle 0, 1\rangle$, and $M_B \in \langle M_{min}, M_{max}\rangle$, i.e., $n(a, e, M_B) \, da \, de \, dM_B$ is the number of binaries with semimajor axis, eccentricity, and mass in $\langle a, a+da\rangle$, $\langle e, e+de\rangle$, and $\langle M_B, M_B+dM_B\rangle$, respectively. The normalization constant then reads

$$A = \begin{cases} \ln^{-1}\left(\dfrac{a_{max}}{a_{min}}\right) \ln^{-1}\left(\dfrac{M_{max}}{M_{min}}\right) & \text{for } \alpha = 1, \\[2ex] \ln^{-1}\left(\dfrac{a_{max}}{a_{min}}\right) \dfrac{1-\alpha}{M_{max}^{1-\alpha} - M_{min}^{1-\alpha}} & \text{for } \alpha \neq 1. \end{cases} \tag{A6}$$

A.1. High-velocity Ejections

The frequency of scattering events of a star with velocity v_c on binaries with number density n_B and semimajor axis a is

$$\nu = \Sigma n_B \, v_c = \frac{2\pi G M_B n_B a}{v_c}, \tag{A7}$$

where we assumed the binary cross-section to be determined by the gravitational focusing, i.e., $\Sigma \approx 2\pi G M_B a / v_c^2$. The mean frequency of ejections can be obtained via integration of Equation (A7) weighted by the distribution function (A5):

$$\bar{\nu}_e = \int_{M_{min}}^{M_{max}} dM_B \int_{a_{min}}^{a_{lim}} da \, \nu(a, M_B) \, n(a, e, M_B). \tag{A8}$$

The upper limit of the semimajor axis, a_{lim}, has to be set such that only interactions that lead to acceleration above the escape velocity from the cluster are considered, i.e.,

$$v_{acc}(a_{lim}) = v_{esc} \approx \sqrt{\frac{2 G M_c}{r_c}} \, , \tag{A9}$$

where r_c is a characteristic radius of the cluster. Combining Equations (A9) and (A4) gives $a_{lim} \approx r_c M_B / M_c$. For the canonical model with initial $M_c = 5400 \, M_\odot$ and $r_c = 0.11 \, \text{pc}$ and for $5 \, M_\odot \leqslant M_B \leqslant 100 \, M_\odot$ we obtain $a_{lim} \gtrsim 100 \, \text{AU}$, which is the upper limit of the semimajor axis distribution used in our numerical integrations. Hence, let us for simplicity assume $a_{lim} = a_{max} = \text{const.}$, which yields

$$\bar{\nu}_e = \begin{cases} \dfrac{2\pi G n_B}{v_c} \dfrac{a_{max} - a_{min}}{\ln(a_{max}/a_{min})} \dfrac{M_{max} - M_{min}}{\ln(M_{max}/M_{min})} & \text{for } \alpha = 1, \\[2.5ex] \dfrac{2\pi G n_B}{v_c} \dfrac{a_{max} - a_{min}}{\ln(a_{max}/a_{min})} \dfrac{1-\alpha}{2-\alpha} \dfrac{M_{max}^{2-\alpha} - M_{min}^{2-\alpha}}{M_{max}^{1-\alpha} - M_{min}^{1-\alpha}} & \text{for } \alpha \neq 1. \end{cases} \tag{A10}$$

Considering an initial OB binary density $n_B \approx 10^5 \, \text{pc}^{-3}$ and velocity dispersion $v_c \approx 10 \, \text{km s}^{-1}$, $a \in \langle 0.1 \, \text{AU}, \, 100 \, \text{AU}\rangle$, and $M_B \in \langle 5 \, M_\odot, \, 100 \, M_\odot\rangle$ with a Salpeter mass function ($\alpha = 2.35$) we obtain $\bar{\nu}_e \approx 0.1 \, \text{Myr}^{-1}$. Hence, the mean time for an OB star to undergo scattering on a massive binary that leads to its ejection from the cluster is $\tau_e \equiv 1/\bar{\nu}_e \approx 10 \, \text{Myr}$ for the canonical model.

A.2. Stellar Collisions

Unlike in the case of stellar ejections, we assume that stellar collisions are caused by binary shrinking due to successive three-body interactions. We further assume all the massive binaries to be hard, i.e., their interaction with the third body leads to the acceleration of the impact star and growth of the binding energy of the binary. The frequency of the events of scattering of a star of mass $M_\star$ on the massive binary is $\nu' = \Sigma v_c n(M_\star) dM_\star$, where $n(M_\star) dM_\star$ is the number of stars of given mass per unit volume. The rate of the energy transfer from the binary to the stars of mass in $\langle M_\star, M_\star + dM_\star\rangle$ is

$$\frac{dE}{dt} \approx \Delta E_\star \nu' = \frac{2\pi G^2 M_B^2 M_\star}{v_c} n(M_\star) dM_\star \, . \tag{A11}$$

The net rate of energy transfer to stars within the whole mass spectrum gives

$$\frac{dE}{dt} \approx \int \frac{2\pi G^2 M_{\rm B}^2 M_\star}{v_{\rm c}} n(M_\star) dM_\star = \frac{2\pi G^2 M_{\rm B}^2 \rho_\star}{v_{\rm c}} \ . \tag{A12}$$

The stars collide when the binary separation at pericentre becomes less than the sum of the stellar radii. In terms of binding energy and with approximation $R_\star(M_1) + R_\star(M_2) \approx R_\star(M_{\rm B})$, the condition for collision reads

$$E_{\rm coll} \approx \frac{1-e}{8} \frac{GM_{\rm B}^2}{R_\star(M_{\rm B})} \ . \tag{A13}$$

The time required to grow the binding energy from the initial value $E_0 \approx (1/8)GM_{\rm B}^2/a_0$ to $E_{\rm coll}$ is

$$t_{\rm coll} \approx (E_0 - E_{\rm coll}) \left| \frac{dE}{dt} \right|^{-1} \approx \frac{v_{\rm c}}{8\pi G \rho_\star} \left(\frac{1-e}{R_\star(M_{\rm B})} - \frac{1}{a_0} \right) \ . \tag{A14}$$

Integration of $t_{\rm coll}$ over the whole parameter space of binaries with the distribution function (A5) gives the characteristic time of stellar collisions:

$$\tau_{\rm coll} \approx \frac{v_{\rm c}}{16\pi G \rho_\star} \int_{a_{\rm min}}^{a_{\rm max}} da \int_{M_{\rm min}}^{M_{\rm max}} dM_{\rm B} \int_0^{1-R_\star(M_{\rm B})/a} de \left(\frac{1-e}{R_\star(M_{\rm B})} - \frac{1}{a_0} \right) n(a, e, M_{\rm B})$$

$$\approx \frac{v_{\rm c}}{16\pi G \rho_\star} \int_{a_{\rm min}}^{a_{\rm max}} da \int_{M_{\rm min}}^{M_{\rm max}} dM_{\rm B} \, A \, a^{-1} M_{\rm B}^{-\alpha} \left(\frac{1}{3R_{\rm B}} - \frac{1}{a} + \frac{R_{\rm B}}{a^2} - \frac{R_{\rm B}^3}{3a^3} \right) \ , \tag{A15}$$

where we denoted $R_{\rm B} \equiv R_\star(M_{\rm B})$; the upper limit on the eccentricity is set such that the binaries are not collisional initially. Assuming $R_{\rm B} \gg a$, we omit the two least significant terms in Equation (A15) and perform the integration over a:

$$\tau_{\rm coll} \approx \frac{A v_{\rm c}}{16\pi G \rho_\star} \int_{M_{\rm min}}^{M_{\rm max}} dM_{\rm B} \, M_{\rm B}^{-\alpha} \left[\frac{1}{3R_{\rm B}} \ln \left(\frac{a_{\rm max}}{a_{\rm min}} \right) + \frac{1}{a_{\rm max}} - \frac{1}{a_{\rm min}} \right] \ . \tag{A16}$$

Finally, using the notation $\tilde{M} \equiv M/M_\odot$ we obtain for $R_\star(M) = R_\odot \tilde{M}^{0.8}$:

$$\tau_{\rm coll} \approx \begin{cases} \dfrac{v_{\rm c}}{16\pi G \rho_\star R_\odot} \left[\dfrac{5}{12} \left(\tilde{M}_{\rm min}^{-0.8} - \tilde{M}_{\rm max}^{-0.8} \right) \ln^{-1} \left(\dfrac{M_{\rm max}}{M_{\rm min}} \right) + \left(\dfrac{R_\odot}{a_{\rm max}} - \dfrac{R_\odot}{a_{\rm min}} \right) \ln^{-1} \left(\dfrac{a_{\rm max}}{a_{\rm min}} \right) \right] & {\rm for} \quad \alpha = 1, \\[2em] \dfrac{v_{\rm c}}{16\pi G \rho_\star R_\odot} \left[\dfrac{1-\alpha}{0.6 - 3\alpha} \dfrac{\tilde{M}_{\rm max}^{0.2-\alpha} - \tilde{M}_{\rm min}^{0.2-\alpha}}{\tilde{M}_{\rm max}^{1-\alpha} - \tilde{M}_{\rm min}^{1-\alpha}} + \left(\dfrac{R_\odot}{a_{\rm max}} - \dfrac{R_\odot}{a_{\rm min}} \right) \ln^{-1} \left(\dfrac{a_{\rm max}}{a_{\rm min}} \right) \right] & {\rm for} \quad \alpha \ne 1. \end{cases} \tag{A17}$$

The canonical model has an initial central density $\rho_\star \approx 2 \times 10^6\, M_\odot\,{\rm pc}^{-3}$, which gives $\tau_{\rm coll} \approx 40\,{\rm Myr}$, i.e., we estimate stellar collisions to be roughly a factor of four less efficient process for OB star removal than three-body scattering. This is somewhat less than what our numerical experiment shows. This discrepancy can be due to several reasons. Most important is probably the fact that stellar collisions may occur sooner due to perturbations that lead to a strong growth of orbital eccentricity. Indeed, the numerical experiments show that most of the collisions occur with $e \gtrsim 0.99$. Hence, the above given derivation can only serve as an order of magnitude estimate.

Altogether, the three-body interactions are expected to decrease the number of OB stars in the canonical model of the ONC by a factor of two on a timescale of $\approx 5\,{\rm Myr}$, which is in accord with the results of the numerical experiment.

REFERENCES

Aarseth, S. 2003, Gravitational *N*-Body Simulations (Cambridge: Cambridge Univ. Press)
Allison, R. J., & Goodwin, S. 2011, MNRAS, 415, 1967
Allison, R. J., Goodwin, S. P., Parker, R. J., Portegies Zwart, S. F., & de Grijs, R. 2010, MNRAS, 407, 1098
Baumgardt, H., & Kroupa, P. 2007, MNRAS, 380, 1589
Baumgardt, H., & Klessen, R. 2011, MNRAS, 413, 1810
Eggleton, P. P., Fitchett, M. J., & Tout, C. A. 1989, ApJ, 347, 998
Geyer, M. P., & Burkert, A. 2001, MNRAS, 323, 988
Glebbeek, E., Gaburov, E., de Mink, S. E., Pols, O. R., & Portegies Zwart, S. F. 2009, A&A, 497, 255
Heggie, D., & Hut, P. 2003, The Million Body Problem (Cambridge: Cambridge Univ. Press)
Hillenbrand, L. A. 1997, AJ, 113, 1733
Hillenbrand, L. A., & Hartmann, L. W. 1998, ApJ, 492, 540

Huff, E. M., & Stahler, S. W. 2006, ApJ, 644, 355
Jeffries, R. D. 2007, MNRAS, 376, 1109
Jones, B. F., & Walker, M. F. 1988, AJ, 95, 1755
Kobulnicky, H. A., & Fryer, C. L. 2007, ApJ, 670, 747
Kraus, S., Weigelt, G., Balega, Y. Y., et al. 2009, A&A, 497, 195
Kroupa, P. 2000, New Astron., 4, 615
Kroupa, P. 2001, MNRAS, 322, 231
Kroupa, P., Aarseth, S., & Hurley, J. 2001, MNRAS, 321, 699
Lang, K. R. 1980, Astrophysical Formulae (Berlin: Springer)
Marks, M., & Kroupa, P. 2012, A&A, 543, A8
Menten, K. M., Reid, M. J., Forbrich, J., & Brunthaler, A. 2007, A&A, 474, 515
Olczak, C., Pfalzner, S., & Eckart, A. 2008, A&A, 488, 1910
Parker, R. J., Goodwin, S. J., Kroupa, P., & Kouwenhoven, M. B. N. 2009, MNRAS, 397, 1577
Pauldrach, A. W. A., Vanbeveren, D., & Hoffmann, T. L. 2011, A&A, 538, A75
Perets, H. B., & Šubr, L. 2012, ApJ, 751, 133

Pflamm-Altenburg, J., & Kroupa, P. 2006, MNRAS, 373, 295
Portegies-Zwart, S. F., Baumgardt, H., Hut, P., Makino, J., & McMillan, S. L. W. 2004, Nature, 428, 724
Sandstrom, K. M., Peek, J. E. G., Bower, G. C., Bolatto, A. D., & Plambeck, R. L. 2007, ApJ, 667, 1161
Šubr, L., Kroupa, P., & Baumgardt, H. 2008, MNRAS, 385, 1673
Suzuki, T. K., Nakasato, N., Baumgardt, H., et al. 2007, ApJ, 668, 435
Tobin, J. J., Hartmann, L., Furezs, G., Mateo, M., & Megeath, S. T. 2009, ApJ, 697, 1103

van Altena, W. F., Lee, J. T., Lee, J.-F., Lu, P. K., & Upgren, A. R. 1988, AJ, 95, 1744
Vitrichenko, É. A. 2002, Astron. Lett., 28, 843
Wilms, J., Nowak, M. A., Pottschmidt, K., Pooley, G. G., & Fritz, S. 2006, A&A, 447, 245
Wilson, T. L., Filges, L., Codella, C., Reich, W., & Reich, P. 1997, A&A, 327, 1177
Zapata, L. A., Schmid-Burgk, J., Ho, P. T. P., Rodriguez, L. F., & Menten, K. M. 2009, ApJ, 704, L45